LANGMUIR

Article

pubs.acs.org/Langmuir

# Rich Variety of Three-Dimensional Nanostructures Enabled by Geometrically Constraining Star-like Block Copolymers

Chao Wang,[†] Yuci Xu,*[,†] Weihua Li,[‡] and Zhiqun Lin*[,§]

[†]Faculty of Materials Science and Chemical Engineering, Ningbo University, Ningbo, Zhejiang 315211, China

[‡]State Key Laboratory of Molecular Engineering of Polymer, Department of Macromolecular Science, Fudan University, Shanghai 200433, China

[§]School of Materials Science and Engineering, Georgia Institute of Technology, Atlanta, Georgia 30332, United States

Ⓢ *Supporting Information*

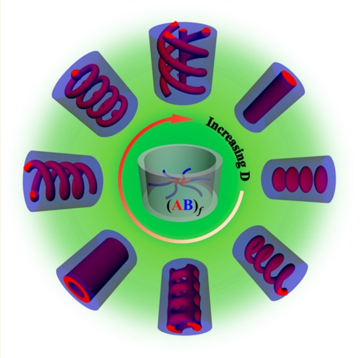

**ABSTRACT:** The influence of star-like architecture on phase behavior of star-like block copolymer under cylindrical confinement differs largely from the bulk (i.e., nonconfinement). A set of intriguing self-assembled morphologies and the corresponding phase diagrams of star-like $(AB)_f$ diblock copolymers with different numbers of arms $f$ (i.e., $f = 3$, 9, 15, and 21) in four scenarios ($\phi_A = 0.3$ and $V_0 > 0$; $\phi_A = 0.3$ and $V_0 < 0$; $\phi_A = 0.7$ and $V_0 > 0$; and $\phi_A = 0.7$ and $V_0 < 0$ (where $\phi_A$ is the volume fraction of A block) and $V_0 < 0$ and $V_0 > 0$ represent that the pore wall of cylindrical confinement prefers the inner A block (i.e., A-preferential) and B block (i.e., B-preferential), respectively) were for the first time scrutinized by employing the pseudospectral method of self-consistent mean-field theory. Surprisingly, a new nanoscopic phase, that is, perforated-lamellae-on-cylinder (denoted PC), was observed in star-like $(AB)_3$ diblock copolymer at $\phi_A = 0.3$ and $V_0 > 0$. With a further increase in $f$, a single lamellae (denoted $L_1$) was found to possess a larger phase region. Under the confinement of A-preferential wall (i.e., $V_0 < 0$) at $\phi_A = 0.3$, PC phase became metastable and its free energy increased as $f$ increased. Quite intriguingly, when $\phi_A = 0.7$ and $V_0 > 0$, where an inverted cylinder was formed in bulk, the PC phase became stable, and its free energy decreased as $f$ increased, suggesting the propensity to form PC phase under this condition. Moreover, in stark contrast to the phase transition of $C_1 \rightarrow L_1 \rightarrow$ PC ($C_1$, a single cylindrical microdmain) at $\phi_A = 0.3$ and $V_0 > 0$, when subjected to the A-preferential wall ($\phi_A = 0.7$), a different phase transition sequence (i.e., $C_1 \rightarrow$ PC $\rightarrow L_1$) was identified due to the formation of a double-layer structure. On the basis of our calculations, the influence of star-like architecture on $(AB)_f$ diblock copolymer under the imposed cylindrical confinement, particularly the shift of the phase boundaries as a function of $f$, was thoroughly understood. These self-assembled nanostructures may hold the promise for applications as lithographic templates for nanowires, photonic crystals, and nanotechnology.

## ■ INTRODUCTION

Due to their unique solution and solid-state properties, star-like block copolymers have received much attention for potential applications in additives, coatings, drug delivery, and supramolecular science.[1−4] Star-like $(AB)_f$ block copolymers are often produced by copolymerization, for example, polystyrene-*block*-polyisoprene (PS-*b*-PI) anions with divinylbenzene (DVB) initiated by *n*-butyllithium.[5] The concentration of diblock anion and the feed ratio of DVB to the diblock anion end dictate the number of arms of the resulting star-like diblock copolymers. Recently, a set of 21-arm star-like block copolymers, including coil−coil poly(acrylic acid)-*b*-polystyrene (PS-*b*-PAA) and coil−rod poly(acrylic acid)-*b*-poly(3-hexylthiophene) (PAA-*b*-P3HT), have been synthesized by either sequential atom transfer radical polymerization (ATRP)[6] or a combination of click chemistry with living polymerization. It is notable that a broad range of functional nanoparticles (e.g., metallic, ferroelectric, magnetic, luminescent, and semiconductor, etc.) with well-controlled dimension and solubility,[7] and 1D inorganic nanonecklace with desired functionalities and properties comprising well-defined nanoscopic building blocks[8] were crafted using these intriguing star-like block copolymers as templates.

Imposing a geometric confinement on block copolymers has been widely recognized as an alternative to creating novel ordered nanostructures, compared to the other means that involve the variation of chemical compositions, architectures, and interactions between immiscible blocks in block copolymers.[9−13] Many efforts in this area have been devoted to exploiting self-assembled yet constrained nanostructures.[14,15] In this context, self-assembly of block copolymers, such as linear AB diblock[16,17] and ABC star[18] in different confined geometries[19,20] including thin-film[21] and cylindrical and hexagonal nanopores, has been intensively investigated theoretically[19,22,23] using self-consistent mean-field theory (SCMFT),[19] Monte Carlo simulation,[11,13,22,24−26] and dissipative particle dynamics calculation,[27] etc. Notably, self-consistent field theory has been extensively employed to explore the formation of nanostruc-

**Received:** May 19, 2016
**Revised:** June 28, 2016
**Published:** July 7, 2016

DOI: 10.1021/acs.langmuir.6b01904
*Langmuir* 2016, 32, 7908−7916

tures under confinement as the corresponding free energy can be readily calculated. Particularly, a powerful spectral method of SCMFT for solving the modified diffusion equation has been developed,[28,29] with which the phase diagram of star-like block copolymers with 1, 3, 5, 9, and 21 arms can be constructed.[29,30] For the 9-arm star-like block copolymer, the phase regions of gyroid and $O^{70}$ phases were found to be larger than those in linear diblock copolymer, and the phase diagrams of star-like block copolymer were asymmetric. When further increasing the number of arms to 21, the phase region of normal morphologies, where the outer block forms the matrix, become larger.[30] It is not surprising that the phase behavior of star-like block copolymer under cylindrical confinement would be largely different between the normal and inverted phase region. We note that there has been very limited study on the phase behavior of $f$-arm star-like block copolymers under cylindrical confinement, especially the difference of phase behavior under confinement when the parameters are located in normal (e.g., $\phi_A = 0.3$ and $\chi N/f = 20$) and inverted (e.g., $\phi_A = 0.7$ and $\chi N/f = 20$) bulk regions. Moreover, the effect of the number of arms $f$ on the phase equilibrium of star-like block copolymer under confinement is of key importance, and the corresponding phase transition sequence may be greatly impacted by the number of arms $f$.

Herein, we report, *for the first time*, the self-assembled morphologies of $f$-arm star-like $(AB)_f$ diblock copolymers (A and B are the inner and outer blocks, respectively) confined in cylindrical nanopore by capitalizing on SCMFT. The influence of the arm number $f$ on the morphology and phase diagram of star-like $(AB)_f$ diblock copolymers in four scenarios, namely, $\phi_A = 0.3$ and $V_0 > 0$; $\phi_A = 0.3$ and $V_0 < 0$; $\phi_A = 0.7$ and $V_0 > 0$; and $\phi_A = 0.7$ and $V_0 < 0$ (the cylindrical pore wall prefers the inner A block at $V_0 < 0$ and attracts the outer B block at $V_0 > 0$), was scrutinized. A rich variety of three-dimensional (3D) phases, including single cylindrical microdomain ($C_1$), stacked disk (Dk), single helix ($H_1$), double helix ($H_2$), alternating toroids and spheres (TS), a double helix winding around a central cylinder ($H_2C$), and single-layer-lamellae ($L_1$), were produced. Phase diagrams of $f$-arm star-like diblock copolymers at different pore diameter $D$ were constructed by comparing the free energy of phases. The free energy difference of morphologies was also depicted. A new nanoscopic phase, perforated-lamellae-on-cylinder (denoted PC), was observed in $(AB)_3$ diblock copolymer at $f = 3$, $\phi_A = 0.3$, and $V_0 > 0$. Rather than PC, a single lamellae ($L_1$) phase possessing a larger phase region was found with further increasing $f$. Under the situation where the pore wall of cylindrical confinement prefers the inner A block (i.e., A-preferential) at $\phi_A = 0.3$, the perforated-lamellae-on-cylinder phase became metastable due to the decrease of effective A block as a thin A layer is formed near the pore wall, and its free energy increased as $f$ increased. Conversely, when star-like $(AB)_f$ block copolymers were at $\phi_A = 0.7$ and $V_0 > 0$, where an inverted cylinder was formed in bulk, PC phase became stable, and its free energy was decreased as $f$ increased, suggesting the propensity to form the perforated-lamellae-on-cylinder. Finally, the emergence and stability of 3D phases in A-preferential wall at $\phi_A = 0.7$ were also explored, where a phase transition sequence of $C_1 \rightarrow$ PC $\rightarrow L_1$ was observed owing to the formation of a double-layer structure. This is in sharp contrast to the phase transition of $C_1 \rightarrow L_1 \rightarrow$ PC at $\phi_A = 0.3$ and $V_0 > 0$.

## ■ THEORY

In this study, a system consisting of incompressible melts of star-like $(AB)_f$ diblock copolymer under cylindrical confinement with pore diameter $D$ is considered, where $f$ is the number of arms. In star-like $(AB)_f$ block copolymer, A and B blocks are the inner and outer blocks, respectively. Each star-like polymer has an equal degree of polymerization $N$, and the degree of polymerization of each arm is assumed to be equal and thus $N/f$. The volume fractions of A blocks and B blocks, $\phi_A$ and $\phi_B$, are defined as $N_A/N$ and $N_B/N$, respectively, where $N_A$ and $N_B$ are the degrees of polymerization of A blocks and B blocks in star-like block copolymer, respectively. The Flory−Huggins interaction parameter $\chi$ is used to characterize the interaction between two dissimilar polymers. The length in SCMFT is expressed in the unit of the radius of gyration of linear polymer, $R_g = (Nb^2/6)^{1/2}$, where $b$ is the Kuhn length. According to many-chain Edwards' theory,[31−35] the free energy functional $F$ for a number of $n$ Gaussian $f$-arm star-like diblock copolymer chains under cylindrical confinement can be given as follows:

$$\begin{aligned}\frac{F}{nk_BT} = -\ln Q + \frac{1}{V}\int \mathrm{d}\mathbf{r}\{\chi N\phi_A(\mathbf{r})\phi_B(\mathbf{r}) - \omega_A(\mathbf{r})\phi_A(\mathbf{r}) \\ - \omega_B(\mathbf{r})\phi_B(\mathbf{r}) - \eta(\mathbf{r})[1 - \phi_A(\mathbf{r}) - \phi_B(\mathbf{r})] \\ + H(\mathbf{r})[\phi_A(\mathbf{r}) - \phi_B(\mathbf{r})]\}\end{aligned} \quad (1)$$

where $\phi_A(\mathbf{r})$ and $\phi_B(\mathbf{r})$ are the monomer densities of A and B blocks, respectively. $Q$ is the partition function of a single polymer (i.e., a star-like diblock copolymer in the present study) interacting with the mean-fields $\omega_A$ and $\omega_B$ produced by the surrounding chains. The spatial integration is restricted to the pore volume $V$. A surface field is then introduced to reflect the preference of the pore wall to different blocks. Similar to our previous work,[16−18] this surface field is chosen to have the following form,

$$\frac{H(\mathbf{r})}{\chi N} = V_0\{\exp[(\sigma + |\mathbf{r}| - R)/\lambda] - 1\} \quad (2)$$

for $R - \sigma \leq |\mathbf{r}| \leq R$, while $H(\mathbf{r}) = 0$ for $|\mathbf{r}| < R - \sigma$. In this work, the distance of surface interaction is chosen as $\sigma = 0.5R_g$, and the decay length $\lambda$ equals $0.5R_g$. $V_0 = 0$ implies that there is no preferential interaction between the pore and the A (or B) block. The pore wall attracts the inner A block at $V_0 < 0$, and prefers the outer B block when $V_0 > 0$.

Minimization of free energy with respect to the monomer densities and the mean fields leads to the following standard mean-field equations for copolymer under confinement.

$$\begin{aligned}&\omega_A(\mathbf{r}) = \chi N\phi_B(\mathbf{r}) + H(\mathbf{r}) + \eta(\mathbf{r}) \\ &\omega_B(\mathbf{r}) = \chi N\phi_A(\mathbf{r}) - H(\mathbf{r}) + \eta(\mathbf{r}) \\ &\phi_A(\mathbf{r}) + \phi_B(\mathbf{r}) = 1 \\ &\phi_A(\mathbf{r}) = \frac{1}{Q}\int_{s\in A} \mathrm{d}s\, q_A(\mathbf{r}, s)\, q_A^{\dagger}(\mathbf{r}, s) \\ &\phi_B(r) = \frac{1}{Q}\int_{s\in B} \mathrm{d}s\, q_B(\mathbf{r}, s)\, q_B^{\dagger}(\mathbf{r}, s) \\ &Q = \frac{1}{V}\int \mathrm{d}\mathbf{r}\, q_K(\mathbf{r}, s)\, q_K^{\dagger}(\mathbf{r}, s)\end{aligned} \quad (3)$$

where $q_K(\mathbf{r},s)$ and $q_K^{\dagger}(\mathbf{r},s)$ (K = A, B) are the end-segment distribution functions, which are proportional to the probability that a polymer segment of contour length $s$ and with one free end has its other end located at $\mathbf{r}$. These distribution functions satisfy the modified diffusion equations.

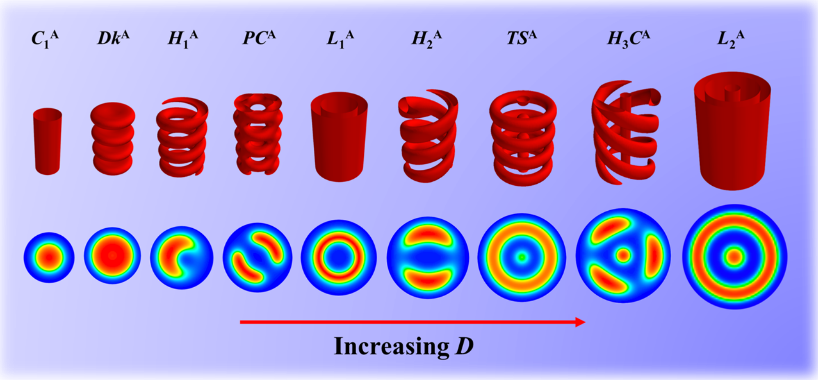

**Figure 1.** Schematic of nanostructured phases of *f*-arm star-like $(AB)_f$ diblock copolymers under cylindrical confinement with the cylindrical pore wall prefering the outer B blocks ($V_0 = 0.2$) at various pore sizes *D*. The parameters chosen in the calculations are $\phi_A = 0.3$ and $\chi N/f = 20$. The upper panels describe the density profiles of inner A blocks, while the matrix composed of B blocks is not shown for clarity. The $C^A$ with a superscript A indicates the normal single cylinder, where the inner A blocks form the cylinder in the outer B block matrix. The same notations are used for the other phases. The lower panels depict the top views of the corresponding phases, where the color ranges from deep red (A-rich regions) to deep blue (B-rich regions).

**Table 1. Summary of Four Types of Notations Used in This Study and the Corresponding Schematic Representations, Where A and B Blocks Are Indicated by Red and Blue, Respectively**[a]

| Scenarios | Notations | $\phi_A$ | $V_0$ | Schematic Representations |
|---|---|---|---|---|
| (I) | $C_1^A$ | 0.3 | 0.2 |  |
| (II) | $\overline{C_1^A}$ | 0.3 | -0.2 | 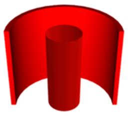 |
| (III) | $\overline{C_1^B}$ | 0.7 | 0.2 | 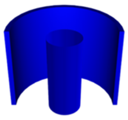 |
| (IV) | $C_1^B$ | 0.7 | -0.2 |  |

[a]. Notably, only a single cylinder was drawn as an example. The $C^A$ with a superscript A indicates the normal single cylinder, where the inner A blocks form the cylinder in the outer B block matrix. The $\overline{C^A}$ with an overbar implies a thin layer of A block is formed near the pore wall. The $\overline{C^B}$ with a superscript B indicates the inverted single cylinder (i.e., the outer B blocks form the cylinder in the inner A block matrix), and an overbar implies a thin layer of B block is formed near the pore wall. The $C^B$ with a superscript B refers to the inverted single cylinder, where the outer B blocks form the cylinder in the inner A block matrix.

$$\frac{\partial q_K(\mathbf{r},s)}{\partial s} = \nabla^2 q_K(\mathbf{r},s) - \omega_K(\mathbf{r})\, q_K(\mathbf{r},s)$$
$$-\frac{\partial q_K^{\dagger}(\mathbf{r},s)}{\partial s} = \nabla^2 q_K^{\dagger}(\mathbf{r},s) - \omega_K(\mathbf{r})\, q_K^{\dagger}(\mathbf{r},s) \qquad (4)$$

The initial conditions are $q_B^{\dagger}(\mathbf{r},1) = 1$, $q_A(\mathbf{r},0) = [q_A^{\dagger}(r,0)]^{f-1}$. The split-step Fourier method was employed to solve the modified diffusion equations for the end-segment distribution functions.[35,36] Similar to our previous work on linear block copolymers under confinement,[16−18] the cross-section of pore is placed in a rectangular cell, which is slightly larger than the pore diameter. The periodic boundary conditions are imposed automatically on the square cell in the split-step Fourier method. The cell is discretized into $N_x \times N_y = 64 \times 64$ and $N_x \times N_y \times N_z = 64 \times 64 \times 64$ for 2D and 3D, respectively. The total chain contour is divided into 1000 segments, which is sufficient to give reasonable results[30] (see discretization test in Supporting Information Figure S1).

## ■ RESULTS AND DISCUSSION

On the basis of our previous study on the phase diagram of 21-arm star-like diblock copolymer in bulk,[30] where the phase diagram is asymmetric due to the topological constraint of star-like architecture, we divide the parameters into two sets. One set is that the inner A blocks have small volume fraction which reflects in the left part of phase diagram. The other set corresponds to the outer B block that has a small volume fraction which is located at the right part of the phase diagram.[30] We note that for linear diblock copolymer under cylindrical confinement, it is clear that there is no difference between these two conditions described above. Interestingly, in contrast, the morphologies of star-like diblock copolymer under confinement are different dramatically as a direct consequence of its star-like architecture. It is also important to note that we concentrated our study that will be discussed below on confinement imposed by narrow cylindrical pores with diameter only a few $L_0$ (i.e., the equilibrium distance between two neighboring cylinders in the hexagonally packed cylindrical structures in bulk) as 3D structures have been observed experimentally for such narrow pore size,[9,10,37] and the morphologies became more complicated at wide pores, making it difficult to determine the stability of the resulting morphologies.

### I. $\phi_A = 0.3$ Where Normal Cylinder Phase Is Formed in Bulk, and $V_0 > 0$ (i.e., the Pore Wall of Cylindrical Confinement Prefers the Outer B Block (B-Preferential)).

In this section, we focus on the outer B block with large volume fraction. To ensure the formation of more interesting morphologies, the parameters chosen were $\phi_A = 0.3$ and $\chi N/f = 20$, which can be readily obtained in experiment by simply controlling the monomer concentration of different blocks.[6] In bulk, hexagonally close-packed cylindrical microdomains of minor A blocks are formed, with a spacing of $L_0 = 2.253R_g$, $1.601R_g$, $1.310R_g$, and $1.130R_g$ between the center of two neighboring A-*block*-containing cylinders for 3-arm, 6-arm, 9-arm, and 12-arm star-like diblock copolymers, respectively. Interestingly, the imposed cylindrical pore confinement with the pore attractive to outer B blocks led to the formation of intriguing 3D either stable or metastable phases, including a single cylindrical microdomain ($C_1^A$; subscript 1 refers to single cylinder), stacked disk ($Dk^A$), single helix ($H_1^A$; subscript 1 refers to single helix), double helix ($H_2^A$; subscript 2 refers to double helix), perforated-lamellae-on-cylinder ($PC^A$), alternating toroids and spheres ($TS^A$), a double helix winding around a central cylinder ($H_2C^A$; subscript 2 refers to double helix), and a triple helix winding around a central cylinder ($H_3C^A$; subscript 3 refers to triple helix) in star-like $(AB)_f$ diblock copolymer with $f = 3$, 6, 9, and 12 by the application of varied random initial fields. Figure 1 shows the side and top views of the morphologies noted above. It is noteworthy that a new stable morphology (i.e., phase), perforated-lamellae-on-cylinder PC (i.e., $PC^A$), which formed in the bulk of self-assembled linear ABC triblock copolymer,[38] was for the first time observed for star-like $(AB)_f$ diblock copolymer under cylindrical confinement. The $C_1^A$ with a superscript A indicates the single cylinder, where the inner A blocks forms the cylinder in the matrix of the outer B block (see Table 1 for four types of notations). The same notations are used for other phases in Figure 1. The stability of each phase and the stable sequence of these phases as a function of the pore size can be identified by carefully comparing the respective free energy with other candidate phases, as summarized in Figure 2. The 3D phase sequence for star-like $(AB)_3$ diblock copolymer, $C_1^A \rightarrow Dk^A \rightarrow H_1^A \rightarrow PC^A \rightarrow H_2^A \rightarrow TS^A \rightarrow H_2C^A/H_3C^A$, is consistent with that of linear AB diblock copolymer under cylindrical confinement; that is, $C_1 \rightarrow Dk \rightarrow H_1 \rightarrow H_2 \rightarrow TS \rightarrow H_1C/H_2C$.[16] It is interesting to note that $PC^A$ was observed as a stable phase in star-like $(AB)_3$ diblock copolymer. The formation of $PC^A$ can be attributed to the fact that $PC^A$ phase needs a larger volume fraction of B block ($\phi_A = 0.3$) than the helix phases. The relative stability of $H_2C^A$ and $H_3C^A$ phases are difficult to determine because the free energy difference is subtle, which correlates well with the result in the literature. We will use $H_3C$ to denote $H_2C$ and $H_3C$ phases later. The appearance of the larger region of $C_1^A$ with increasing $f$ can be ascribed to the star-like architecture of diblock copolymer, which is similar to the structure of imposed cylindrical nanopores. Notably, 2D phases, $L_1$ and $L_2$, were found as stable morphologies and possessed a large phase region with a further increase of $f$ (Figure 2). The phase transition and free energy behaviors of 15- and 21-arm star-like diblock copolymers are expected to be similar to those of 12-arm star-like diblock copolymer and thus are not shown here.

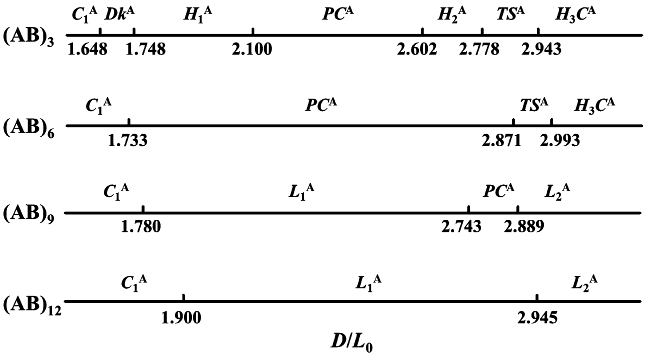

**Figure 2.** Phase diagrams for $f$-arm star-like $(AB)_f$ diblock copolymers ($f = 3$, 6, 9, 12) with $\phi_A = 0.3$, $\chi N/f = 20$, and $V_0 = 0.2$ (i.e., B-preferential wall) confined in cylindrical pores of various diameters $D$ measured in units of the corresponding center-to-center distance, $L_0$, between cylinders in the bulk.

To gain a better understanding on these phase behaviors, the free energies of 3-arm, 6-arm, 9-arm, and 12-arm star-like $(AB)_f$ diblock copolymers as a function of cylindrical pore size at the fixed $\chi N/f = 20$ and $\phi_A = 0.3$ for different stable and metastable phases were calculated and compared, as shown in Figure S2. For clarity, a free energy difference, $\Delta F$, defined as the value of the free energy of a phase subtracted by that of $L_1^A$, was used to identify the relative stability among all these phases. As evidenced in Figure S2a, $PC^A$ has a lower free energy in the diameter ($D/L_0$) range from 2.1 to 2.56. This phase region became wider with increasing $f$ (Figure S2b). Figure S3c shows that a 2D $L_1^A$ phase has the lowest free energy when the number of arms $f$ is 6. The emergence of $L_1^A$ can be ascribed to the fact that the large volume fraction of B block ($\phi_B = 0.7$) leads to the compression of polymer chain in $Dk^A$, $H_1^A$, and $H_2^A$ phases. Particularly, with the increase of $f$, the compression of chain became more important as the chain density increased with larger arms. Consequently, $L_1^A$ possesses a larger phase region with a further increase of $f$, as clearly shown in Figure S2.

### II. $\phi_A = 0.3$ Where Normal Cylinder Phase Is Formed in Bulk, and $V_0 < 0$ (i.e., the Pore Wall of Cylindrical Confinement Prefers the Inner A Block (A-Preferential)).

It is well-known that the pore wall interaction exerts profound influence on the formation of nanostructures,[16] which was clearly manifested in the self-assembled phases under cylindrical nanopores with A-preferential wall (Figure 3). In comparison to the structures formed in a B-preferential wall as discussed above, a thin layer of A block formed near the cylindrical pore

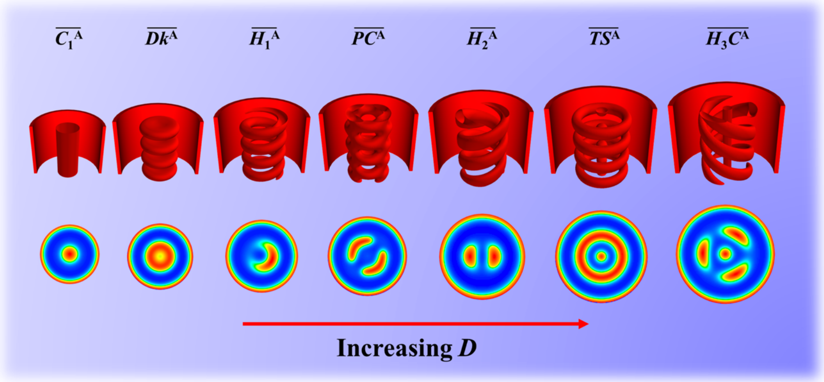

**Figure 3.** Schematic of nanostructured phases of *f*-arm star-like $(AB)_f$ diblock copolymer under cylindrical confinement with the pore wall prefering the inner A block ($V_0 = -0.2$) at various pore sizes *D*. The parameters chosen in the calculations are $\phi_A = 0.3$ and $\chi N/f = 20$. The upper panels compare the density profiles of inner A blocks, while the matrix composed of B block is not shown for clarity. The $\overline{C^A}$ with a superscript A indicates the normal single cylinder, where the inner A blocks form the cylinder in the outer B block matrix (an overbar implies a thin layer of A block formed near the pore wall). The same notations are used for the other phases. The lower panels illustrate the top views of the corresponding phases, where the color ranges from deep red (A-rich regions) to deep blue (B-rich regions).

wall, where $\overline{C_1^A}$, $\overline{Dk^A}$, $\overline{H_1^A}$, $\overline{H_2^A}$, $\overline{TS^A}$, and $\overline{H_3C^A}$ with an overbar were used to designate these phases.[16] It is not surprising that a thin layer was formed near the pore as the pore attracts A blocks. The stable and metastable 3D phases and their phase transition sequence were summarized in Figure 4. It is worth noting that the 3D phase sequences in the A-attractive wall, that is, $\overline{C_1^A} \to \overline{Dk^A} \to \overline{H_1^A} \to \overline{H_2^A} \to \overline{TS^A} \to \overline{H_3C^A}$, was different from that in the B-attractive wall case ($C_1^A \to Dk^A \to H_1^A \to PC^A \to H_2^A \to TS^A \to H_3C^A$). The $\overline{PC^A}$ and $\overline{L_1^A}$ phases did not appear in the stable phase sequence. These two phases were metastable, and their arrangement became more frustrated due to the decrease of effective volume fraction of A blocks as some A blocks formed a thin layer near the pore wall. We note that the phase transition sequences were the same with only a slight shift toward larger $D/L_0$ as *f* increased, which can be ascribed to the restriction of star-like architecture. The corresponding free energies of star-like $(AB)_3$, $(AB)_9$, $(AB)_{15}$, and $(AB)_{21}$ diblock copolymers were summarized in Figure S3. For clarity, a free energy relative to a selected reference phase (i.e., $\overline{PC^A}$), $\Delta F$, was plotted to demonstrate the relative stability of these phases. The free energy of $\overline{C_1^A}$ and $\overline{Dk^A}$ were not shown in Figure S3 as the $\overline{PC^A}$ phases cannot be observed in such a narrow nanopore, so that the free energy difference cannot be obtained. Strikingly, the free energy of $\overline{PC^A}$ phase increased as *f* increased, and $\overline{L_1^A}$ phase cannot be observed in the calculations. The increase of $\overline{PC^A}$ free energy may be due to the fact that it was energetically unfavorable for the outer B blocks to form the perforated area, in which the polymer arrangement was similar to the inverted cylinder morphologies.[30] Consequently, high free energy was achieved, and increased as *f* increased.

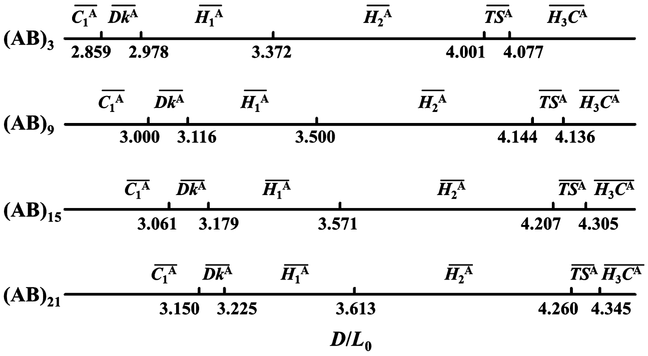

**Figure 4.** Phase diagrams of *f*-arm star-like diblock copolymers with $\phi_A = 0.3$ and $\chi N/f = 20$ ($f = 3$, 9, 15, and 21) confined in cylindrical pores of varied diameter *D* measured in units of the corresponding center-to-center distance, $L_0$, between cylinders in the bulk. $V_0 = -0.2$ reflects that the pore wall prefers the inner A blocks.

**III. $\phi_A = 0.7$ Where Inverted Cylinder Phase Is Formed in Bulk, and $V_0 > 0$ (B-Preferential Wall).** In this and the following sections, we turn our attention to the formation of inverted phases. The volume fraction of $\phi_A = 0.7$ and the repulsive interaction $\chi N/f = 20$ were chosen. The strength parameter of the surface field was selected as $V_0 = 0.2$ to offer strong attraction to B blocks and strong repulsion to A blocks. The corresponding bulk cylinder-to-cylinder distances, $L_0$, of star-like $(AB)_3$, $(AB)_9$, $(AB)_{15}$, and $(AB)_{21}$ diblock copolymers are 2.554, 1.501, 1.173, and 0.993, respectively. First, we considered the phases that form in a B-attractive pore wall, and the results for A-preferential wall will be discussed in section IV. The stable and metastable nanostructured phases found under this condition are shown in Figure 5. The $\overline{C_1^B}$, $\overline{Dk^B}$, $\overline{H_1^B}$, $\overline{H_2^B}$, $\overline{PC^B}$, $\overline{TS^B}$, and $\overline{H_3C^B}$, in which a superscript B refers to the inverted phases, were obtained, where the outer B blocks form C, Dk, $H_1$, $H_2$, TS, and $H_3C$ phases because of the spontaneous curvature. An overbar signifies a thin layer of the B blocks forms near the pore wall.

Similarly, the stability of each phase as well as their stable phase sequences as a function of the pore size can be achieved by carefully comparing the respective free energy with other candidate phases. The corresponding phase transition sequences of these phases with *f* are summarized in Figure 6. Clearly, the phase region of $\overline{PC^B}$ became wider as *f* increased. For star-like $(AB)_3$ diblock copolymer, the phase transition sequence of $\overline{C_1^B} \to \overline{Dk^B} \to \overline{H_1^B} \to \overline{H_2^B} \to \overline{PC^B} \to \overline{H_2^B} \to \overline{TS^B} \to \overline{H_3C^B}$ was

DOI: 10.1021/acs.langmuir.6b01904
*Langmuir* 2016, 32, 7908−7916

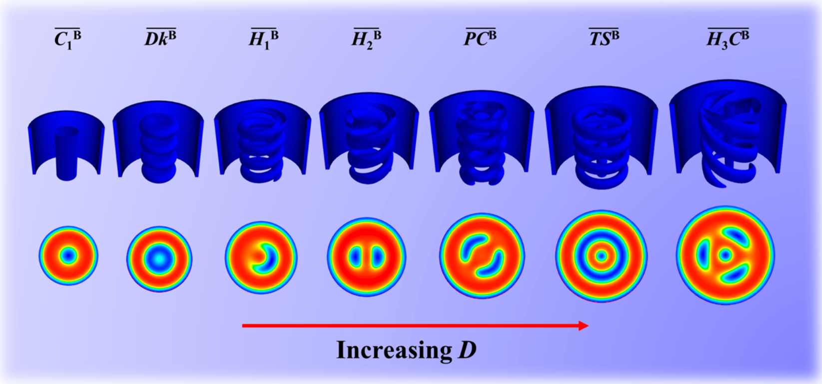

**Figure 5.** Schematic of nanostructured phases of $f$-arm star-like $(AB)_f$ diblock copolymers under cylindrical confinement with the pore wall prefering the outer B blocks ($V_0 = 0.2$) at various pore sizes $D$. The parameters chosen in the calculations are $\phi_A = 0.7$ and $\chi N/f = 20$. The upper panels depict the density profiles of the outer B blocks (deep blue), while the matrix composed of A block is not shown for clarity, which can be clearly observed in the corresponding top view. The $\overline{\mathrm{C}}^{\mathrm{B}}$ with a superscript B indicates the inverted single cylinder, where the outer B blocks form the cylinder in the inner A block matrix. An overbar implies a thin layer of B block formed near the pore wall. The same notations are used for the other phases. The lower panels display the top views of the corresponding nanostructures, where the color ranges from deep red (A-rich regions) to deep blue (B-rich regions).

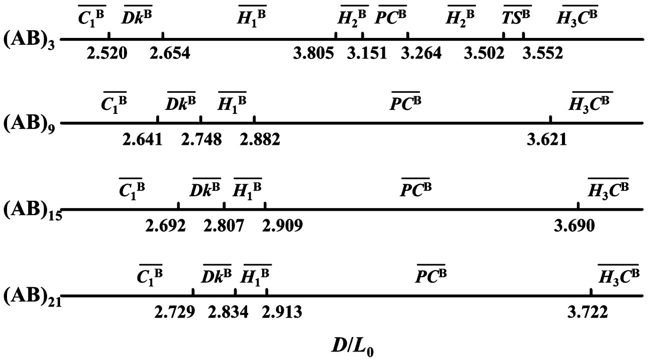

**Figure 6.** Stable sequences of phases formed in $f$-arm star-like $(AB)_f$ diblock copolymers ($f$ = 3, 9, 15, and 21) at $\phi_A = 0.7$, $\chi N/f = 20$, and $V_0 = 0.2$, where the pore wall prefers the B blocks, under the cylindrical confinement with the varied diameter $D$ of nanopores. The $D$ was normalized by the corresponding bulk cylinder-to-cylinder distance, $L_0 = 2.554R_g$, $1.509R_g$, $1.174R_g$, and $0.993R_g$ for 3-arm, 9-arm, 15-arm, and 21-arm star-like diblock copolymers, respectively.

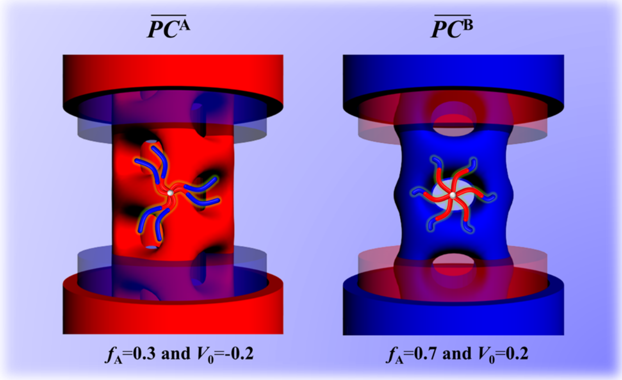

**Figure 7.** Schematic illustration of the arrangement of star-like $(AB)_f$ diblock copolymer in $\overline{\mathrm{PC}}^{\mathrm{A}}$ and $\overline{\mathrm{PC}}^{\mathrm{B}}$ phases. For clarity, only parts of the corresponding matrix are shown. The perforated area in $\overline{\mathrm{PC}}^{\mathrm{A}}$ is filled with the outer B blocks (blue), where the outer B blocks are compressed and the inner A blocks are stretched to adjust this chain arrangement, which is similar to that of an inverted cylinder in the literature.[30] For the $\overline{\mathrm{PC}}^{\mathrm{A}}$ phase, the inner A blocks form the perforated area, which is energetically favorable for the star-like architecture. Only six representative arms are shown for clarity.

observed, where $\overline{\mathrm{PC}}^{\mathrm{B}}$ possesses a very tiny phase region. It is interesting to note that when further increasing $f$, the phase transition sequence changed to $\overline{\mathrm{C}_1}^{\mathrm{B}} \rightarrow \overline{\mathrm{Dk}}^{\mathrm{B}} \rightarrow \overline{\mathrm{H}_1}^{\mathrm{B}} \rightarrow \overline{\mathrm{PC}}^{\mathrm{B}} \rightarrow \overline{\mathrm{H}_3\mathrm{C}}^{\mathrm{B}}$, where $\overline{\mathrm{PC}}^{\mathrm{B}}$ has a large phase region and its phase region increased as $f$ increased (Figure 6). For linear diblock copolymer AB (i.e., $f = 1$), the phase transition sequence at $\phi_A = 0.3$ for the case of wall attracting A blocks is exactly identical to that with $\phi_A = 0.7$ for the case of wall attracting B blocks. $\mathrm{PC}^{\mathrm{A}}$ was a metastable phase, and its free energy increased as $f$ increased. In stark contrast, $\overline{\mathrm{PC}}^{\mathrm{B}}$ was, however, found to be more stable (Figure 6). This is not surprising as the perforated area in $\mathrm{PC}^{\mathrm{B}}$ was formed by the inner A blocks (Figure 7), which matched well with the star-like architecture, thereby leading to the decrease of free energy. Nonetheless, this mechanism was clearly demonstrated in the chain arrangement of $\overline{\mathrm{PC}}^{\mathrm{A}}$ and $\overline{\mathrm{PC}}^{\mathrm{B}}$ (Figure 7). In addition, the phase region of $\overline{\mathrm{H}_1}^{\mathrm{B}}$ and $\mathrm{H}_3\mathrm{C}^{\mathrm{B}}$ became narrower as $f$ increased. This observation was consistent with the results that PC has a larger phase region.

In order to understand the phase diagram shown in Figure 6, the free energies of the stable and metastable phases were summarized in Figure S4. A free energy difference, $\Delta F$, defined as the value of free energy of a phase subtracted by that of $\overline{\mathrm{PC}}^{\mathrm{B}}$, was used to evaluate the relative stability among these phases. Since $\overline{\mathrm{PC}}^{\mathrm{B}}$ cannot be formed in such a narrow pore, the free energy difference between $\overline{\mathrm{C}_1}^{\mathrm{B}}$ phase and $\overline{\mathrm{PC}}^{\mathrm{B}}$ cannot be obtained. Thus, the free energy of $\overline{\mathrm{C}_1}^{\mathrm{B}}$ was not shown in Figure S4. However, the phase transition can be obtained by comparing the free energy between $\overline{\mathrm{C}_1}^{\mathrm{B}}$ and $\overline{\mathrm{Dk}}^{\mathrm{B}}$ phases. For the free energy of 3-arm star-like $(AB)_f$ diblock copolymer ($f$ = 3) (Figure S4a), the free energy of $\overline{\mathrm{PC}}^{\mathrm{B}}$ was always high.

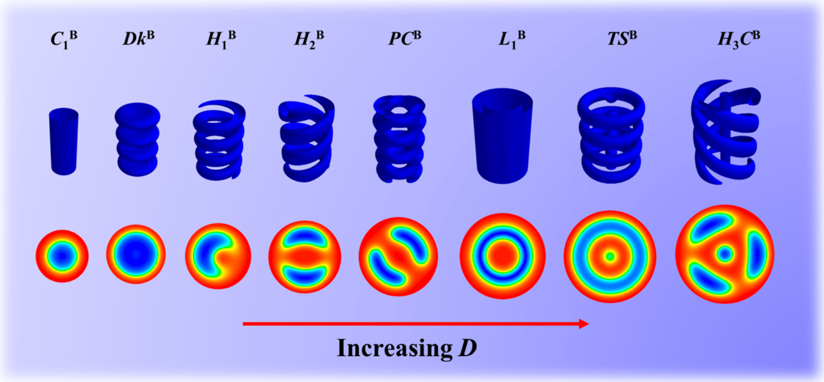

**Figure 8.** Schematic of nanostructured phases of $f$-arm star-like $(\mathrm{AB})_f$ diblock copolymers under cylindrical confinement with the pore wall prefering the inner A blocks ($V_0 = -0.2$) at various pore sizes $D$. The parameters chosen in the calculations are $\phi_{\mathrm{A}} = 0.7$ and $\chi N/f = 20$. The upper panels describe the density profiles of the outer B blocks, while the matrix composed of inner A block is not shown for clarity. The $\mathrm{C^B}$ with a superscript B indicates the inverted single cylinder, where the outer B blocks form the cylinder in the inner A block matrix. The same notations are used for the other phases. The lower panels depict the top views of the corresponding phases, where the color ranges from deep red (A-rich regions) to deep blue (B-rich regions).

However, as $f$ increased to 9, the free energy of $\overline{\mathrm{PC}}^{\mathrm{B}}$ decreased and its phase region became wider (Figure S4b). A further increase of $f$ led to the unstable helix. As a result, these phases cannot be observed, even as metastable phases (Figure S4c,d). On the basis of the free energy difference, the phase transition sequences described in Figure 6 were thus fully understood.

**IV. $\phi_{\mathrm{A}}$ = 0.7 Where Inverted Cylinder Phase Is Formed in Bulk, and $V_0 < 0$ (A-Preferential Wall).** For the case in which the pore wall preferentially attracts the inner A blocks at $\phi_{\mathrm{A}} = 0.7$, a thin layer near the pore wall was not formed (Figure 8). Notably, a 2D lamellae phase ($\mathrm{L_1^B}$) at the larger number of arms (i.e., $f > 4$) was obtained. To reveal the relative stability of these stable and metastable phases, the phase diagram was shown in Figure 9. Interestingly, the largest number of arms $f$ calculated in Figure 9 was only 6. This is because the 3D phases, such as disk and helix, were unstable when $f$ was larger than 6 (Figure S5). $\mathrm{L_1^B}$ showed a larger phase region, especially when $f$ was larger. On the basis of this trend, the phase transition sequences of larger $f$ are expected to be similar to that of 6-arm star-like diblock copolymer, where $\mathrm{L_1^B}$ was found to be most stable. To clearly demonstrate the shift of phase transition as a function of $f$, the phase diagrams of 3-, 4-, 5-, and 6- (not 3-, 9-, 15-, and 21-) arm star-like diblock copolymers were calculated. The formation of $\mathrm{L_1^B}$ can be ascribed to the fact that a larger volume fraction of outer B block ($\phi_{\mathrm{B}} = 0.3$) resulted in the compression of polymer chain in PC, helix, and TS phases. However, for the phases formed in the B-preferential wall cases, the effective volume fraction of B block decreased as a thin B layer was formed near the pore wall (Figure 5), leading to the formation of $\overline{\mathrm{PC}}^{\mathrm{B}}$ phase. The phases at $\phi_{\mathrm{A}} = 0.7$ and $V_0 = -0.2$ (A-preferential wall) exhibited a $\mathrm{C_1^B} \rightarrow \mathrm{PC^B} \rightarrow \mathrm{L_1^B}$ transition sequence, where $\mathrm{L_1^B}$ phase was stable at the lager pore wall. This contrasts the sequence of $\mathrm{C_1^A} \rightarrow \mathrm{L_1^A} \rightarrow \mathrm{PC^A}$ in the case where $\phi_{\mathrm{A}} = 0.3$ and $V_0 = 0.2$ (B-preferential wall). The emergence of $\mathrm{L_1^B}$ at the larger pore size is due to the formation of a double-layer structure (Figure S6). For the $\mathrm{L_1^A}$ phase form in the case of $\phi_{\mathrm{A}} = 0.3$ and B-preferential wall, the star-like diblock copolymer preferred a single-layer structure (Figure S6). Consequently, $\mathrm{L_1^A}$ became metastable as the pore size increased. The phase transitions were clearly revealed in the free energy difference $\Delta F$ obtained by subtracting the free energy with that of $\mathrm{L_1^B}$ (Figure S7). Clearly, the free energy of $\mathrm{L_1^B}$ decreased as $f$ increased. It is interesting to note that some 3D phases at $f > 5$, that is, $\mathrm{Dk^B}$, $\mathrm{H_1^B}$, $\mathrm{H_2^B}$, $\mathrm{TS^B}$, and $\mathrm{H_3C^B}$ phases, were not shown in Figure S7, as these phases were unstable due to higher free energy.

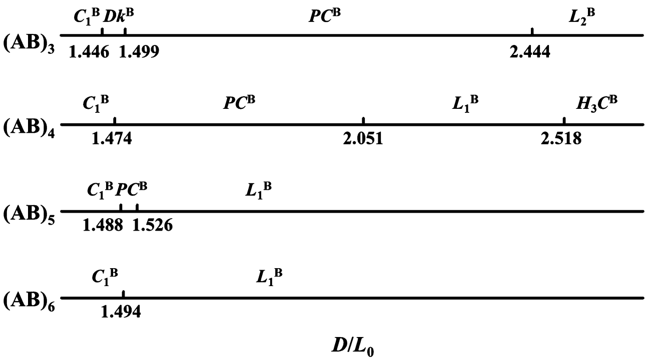

**Figure 9.** Stable sequences of phases formed in $f$-arm star-like $(\mathrm{AB})_f$ diblock copolymers ($f$ = 3, 4, 5, and 6) at $\phi_{\mathrm{A}} = 0.7$, $\chi N/f = 20$, and $V_0 = -0.2$, where the pore wall prefers the A blocks, under the cylindrical confinement with the varied diameter $D$ of nanopores. $D$ was normalized by the corresponding bulk cylinder-to-cylinder distance, $L_0 = 2.554R_g$, $2.232R_g$, $2.007R_g$, and $1.838R_g$ for 3-arm, 4-arm, 5-arm, and 6-arm star-like diblock copolymers, respectively. The phase diagrams with $f > 6$ were not shown (shown in Figure S5 instead) as 3D phases cannot be obtained even as metastable phases.

## ■ CONCLUSIONS

In summary, the emergency and stability of 3D phases in $f$-arm star-like $(\mathrm{AB})_f$ diblock copolymers under cylindrical confinement were systematically explored by the self-consistent mean-field theory calculations. Four scenarios, that is, $\phi_{\mathrm{A}} = 0.3$ and $V_0 = -0.2$ (A-preferential wall), $\phi_{\mathrm{A}} = 0.3$ and $V_0 = 0.2$ (B-preferential wall), $\phi_{\mathrm{A}} = 0.7$ and $V_0 = -0.2$, and $\phi_{\mathrm{A}} = 0.7$ and $V_0$= 0.2, were, for the first time, scrutinized to reveal the influence of asymmetry (i.e., asymmetric volume fraction) on the phase behaviors of star-like $(\mathrm{AB})_f$ diblock copolymer under cylindrical confinement. An exciting variety of 3D phases, including a single cylindrical microdomain ($\mathrm{C_1}$), stacked disk (Dk), single helix ($\mathrm{H_1}$), double helix ($\mathrm{H_2}$), alternating toroids and spheres (TS), and a double helix winding around a central cylinder ($H_2C$), were identified. Moreover, the corresponding free energy difference was obtained to show the influence of the number of arms $f$ on the shift of phase boundaries. Notably, a new phase, perforated-lamellae-on-cylinder (PC), was yielded in star-like $(AB)_3$ diblock copolymer at $\phi_A = 0.3$ and $V_0 > 0$. Due to the packing frustration of the PC phase where the perforated area comprised the outer B blocks, a single lamellae ($L_1^A$) phase possessed a larger phase region as $f$ increased. In addition, under the A-preferential wall confinement at $\phi_A = 0.3$, $\overline{PC}^A$ phase became metastable due to the decrease of effective A blocks as a thin A layer was formed near the pore wall, and its free energy increased as $f$ increased. In sharp contrast, when star-like $(AB)_f$ diblock copolymers were at $\phi_A = 0.7$ and $V_0 > 0$ where the inverted cylinder was formed in bulk, $\overline{PC}^B$ was stable and its free energy decreased as $f$ increased, signifying the propensity to form the $\overline{PC}^B$ phase under this condition. Finally, the self-assembled 3D phases of star-like $(AB)_f$ diblock copolymer in the case of A-preferential wall ($V_0 < 0$) and $\phi_A = 0.7$ were also explored, where a phase transition sequence of $C_1^B \rightarrow PC^B \rightarrow L_1^B$ was found. This may be due to the formation of a double-layer structure, thereby leading to the emergence of $L_1{}^A$ phase at the larger pore size. For $\phi_A = 0.3$ and $V_0 > 0$, a $C_1^A \rightarrow L_1^A \rightarrow PC^A$ sequence, however, was yielded. Clearly, our calculations provided a fundamental understanding on the shift of phase boundaries as a function of $f$ and on the influence of star-like architecture on phase behavior of star-like $(AB)_f$ diblock copolymer under cylindrical confinement. We envision that such intriguing self-assembled nanostructures derived from the geometrically constrained star-like diblock copolymers may be exploited as unique lithographic templates for creating complex inorganic functional materials and devices.[39]

## ■ ASSOCIATED CONTENT

### Ⓢ Supporting Information

The Supporting Information is available free of charge on the ACS Publications website at DOI: 10.1021/acs.langmuir.6b01904.

> Phase diagram of 21-arm star-like $(AB)_f$ diblock copolymer, free engery comparisons between different phases, stable sequences of phases, and schematic illustration of $(Ab)_f$ diblock copolymer chain, (PDF)

## ■ AUTHOR INFORMATION

### Corresponding Authors

*(Y.X.) E-mail: xuyuci@nbu.edu.cn.
*(Z.L.) E-mail: zhiqun.lin@mse.gatech.edu.

### Notes

The authors declare no competing financial interest.

## ■ ACKNOWLEDGMENTS

We gratefully acknowledge the funding support from the National Natural Science Foundation of China (Grant 21304051), Zhejiang Xinmiao Program (Grant 2014R405090; C.W.), and K. C. Wong Magna Foundation at Ningbo University. This work was also supported by the Air Force Office of Scientific Research (AFOSR; Grant FA9550-16-1-0187).

## ■ REFERENCES

(1) Char, K.; Frank, C. W.; Gast, A. P. Fluorescence Studies of Polymer Adsorption 0.3. Adsorption of Pyrene-End-Labeled Poly(Ethylene Glycol) on Colloidal Polystyrene Particles. *Langmuir* **1989**, *5*, 1335−1340.

(2) Char, K.; Frank, C. W.; Gast, A. P. Fluorescence Studies of Polymer Adsorption 0.2. A Simple-Model Describing Adsorbed Polymer Rearrangement. *Langmuir* **1989**, *5*, 1096−1105.

(3) Char, K.; Frank, C. W.; Gast, A. P. Consideration of Hydrophobic Attractions in End-to-End Cyclization. *Macromolecules* **1989**, *22*, 3177−3180.

(4) Hatada, K.; Nishiura, T.; Kitayama, T.; Ute, K. Toward Uniform Polymer Architecture through Stereospecific Living Polymerization and Chromatographic Separation Technique. *Macromol. Symp.* **1997**, *118*, 135−141.

(5) Uchida, S.; Ichimura, A.; Ishizu, K. Preparation and Microphase-Separated Structures of (Ab)(N) Star-Block Copolymers Composed of Symmetric Diblock Arms. *Polymer* **1999**, *40*, 1019−1023.

(6) Pang, X. C.; Zhao, L.; Akinc, M.; Kim, J. K.; Lin, Z. Q. Novel Amphiphilic Multi-Arm, Star-Like Block Copolymers as Unimolecular Micelles. *Macromolecules* **2011**, *44*, 3746−3752.

(7) Pang, X. C.; Zhao, L.; Han, W.; Xin, X. K.; Lin, Z. Q. A General and Robust Strategy for the Synthesis of Nearly Monodisperse Colloidal Nanocrystals. *Nat. Nanotechnol.* **2013**, *8*, 426−431.

(8) Xu, H.; Xu, Y.; Pang, X.; He, Y.; Jung, J.; Xia, H.; Lin, Z. A General Route to Nanocrystal Kebabs Periodically Assembled on Stretched Flexible Polymer Shish. *Sci. Adv.* **2015**, *1*, e1500025.

(9) Xiang, H. Q.; Shin, K.; Kim, T.; Moon, S. I.; McCarthy, T. J.; Russell, T. P. Block Copolymers under Cylindrical Confinement. *Macromolecules* **2004**, *37*, 5660−5664.

(10) Xiang, H.; Shin, K.; Kim, T.; Moon, S. I.; McCarthy, T. J.; Russell, T. P. From Cylinders to Helices Upon Confinement. *Macromolecules* **2005**, *38*, 1055−1056.

(11) Yu, B.; Sun, P. C.; Chen, T. H.; Jin, Q. H.; Ding, D. T.; Li, B. H.; Shi, A.-C. Confinement-Induced Novel Morphologies of Block Copolymers. *Phys. Rev. Lett.* **2006**, *96*, 138306.

(12) Yu, B.; Sun, P.; Chen, T.; Jin, Q.; Ding, D.; Li, B.; Shi, A.-C. Self-Assembled Morphologies of Diblock Copolymers Confined in Nanochannels: Effects of Confinement Geometry. *J. Chem. Phys.* **2007**, *126*, 204903.

(13) Yu, B.; Jin, Q. H.; Ding, D. T.; Li, B. H.; Shi, A. C. Confinement-Induced Morphologies of Cylinder-Forming Asymmetric Diblock Copolymers. *Macromolecules* **2008**, *41*, 4042−4054.

(14) Yan, N.; Liu, H.; Zhu, Y.; Jiang, W.; Dong, Z. Entropy-Driven Hierarchical Nanostructures from Cooperative Self-Assembly of Gold Nanoparticles/Block Copolymers under Three-Dimensional Confinement. *Macromolecules* **2015**, *48*, 5980−5987.

(15) Zhu, Y.; Jiang, W. Self-Assembly of Diblock Copolymer Mixtures in Confined States: A Monte Carlo Study. *Macromolecules* **2007**, *40*, 2872−2881.

(16) Li, W. H.; Wickham, R. A. Self-Assembled Morphologies of a Diblock Copolymer Melt Confined in a Cylindrical Nanopore. *Macromolecules* **2006**, *39*, 8492−8498.

(17) Li, W. H.; Wickham, R. A.; Garbary, R. A. Phase Diagram for a Diblock Copolymer Melt under Cylindrical Confinement. *Macromolecules* **2006**, *39*, 806−811.

(18) Xu, Y.; Li, W.; Qiu, F.; Yang, Y.; Shi, A.-C. Self-Assembly of Abc Star Triblock Copolymers under a Cylindrical Confinement. *J. Phys. Chem. B* **2009**, *113*, 11153−11159.

(19) Chen, P.; Liang, H. J.; Shi, A. C. Microstructures of a Cylinder-Forming Diblock Copolymer under Spherical Confinement. *Macromolecules* **2008**, *41*, 8938−8943.

(20) Deng, R.; Li, H.; Liang, F.; Zhu, J.; Li, B.; Xie, X.; Yang, Z. Soft Colloidal Molecules with Tunable Geometry by 3d Confined Assembly of Block Copolymers. *Macromolecules* **2015**, *48*, 5855−5860.

(21) Li, W.; Liu, M.; Qiu, F.; Shi, A.-C. Phase Diagram of Diblock Copolymers Confined in Thin Films. *J. Phys. Chem. B* **2013**, *117*, 5280−5288.

(22) Chen, P.; He, X.; Liang, H. Effect of Surface Field on the Morphology of a Symmetric Diblock Copolymer under Cylindrical Confinement. *J. Chem. Phys.* **2006**, *124*, 104906.

(23) Wang, X. H.; Li, S. B.; Chen, P.; Zhang, L. X.; Liang, H. J. Microstructures of Lamella-Forming Diblock Copolymer Melts under Nanorod-Array Confinements. *Polymer* **2009**, *50*, 4964−4972.

(24) Wang, Z.; Li, B. H.; Jin, Q. H.; Ding, D. T.; Shi, A. C. Self-Assembly of Cylinder-Forming Aba Triblock Copolymers under Cylindrical Confinement. *Macromol. Theory Simul.* **2008**, *17*, 301−312.

(25) Yang, R.; Li, B.; Shi, A.-C. Phase Behavior of Binary Blends of Diblock Copolymer/Homopolymer Confined in Spherical Nanopores. *Langmuir* **2012**, *28*, 1569−1578.

(26) Chi, P.; Wang, Z.; Li, B.; Shi, A.-C. Soft Confinement-Induced Morphologies of Diblock Copolymers. *Langmuir* **2011**, *27*, 11683−11689.

(27) Li, X.; Tang, Y.-H.; Liang, H.; Karniadakis, G. E. Large-Scale Dissipative Particle Dynamics Simulations of Self-Assembled Amphiphilic Systems. *Chem. Commun.* **2014**, *50*, 8306−8308.

(28) Matsen, M. W.; Schick, M. Stable and Unstable Phases of a Diblock Copolymer Melt. *Phys. Rev. Lett.* **1994**, *72*, 2660−2663.

(29) Matsen, M. W.; Schick, M. Microphase Separation in Starblock Copolymer Melts. *Macromolecules* **1994**, *27*, 6761−6767.

(30) Xu, Y. C.; Li, W. H.; Qiu, F.; Lin, Z. Q. Self-Assembly of 21-Arm Star-Like Diblock Copolymer in Bulk and under Cylindrical Confinement. *Nanoscale* **2014**, *6*, 6844−6852.

(31) Edwards, S. F. Statistical Mechanics of Polymers with Excluded Volume. *Proc. Phys. Soc., London* **1965**, *85*, 613.

(32) Helfand, E. Theory of Inhomogeneous Polymers - Fundamentals of Gaussian Random-Walk Model. *J. Chem. Phys.* **1975**, *62*, 999−1005.

(33) Fredrickson, G. H. *The Equilibrium Theory of Inhomogeneous Polymers*; Oxford University Press: Oxford, U.K., 2006.

(34) Shi, A. C. *Development in Block Copolymer Science and Technology*; John Wiley & Sons: New York, 2004.

(35) Tzeremes, G.; Rasmussen, K. Ø.; Lookman, T.; Saxena, A. Efficient Computation of the Structural Phase Behavior of Block Copolymers. *Phys. Rev. E: Stat. Phys., Plasmas, Fluids, Relat. Interdiscip. Top.* **2002**, *65*, 041806.

(36) Rasmussen, K. O.; Kalosakas, G. Improved Numerical Algorithm for Exploring Block Copolymer Mesophases. *J. Polym. Sci., Part B: Polym. Phys.* **2002**, *40*, 1777−1783.

(37) Xiang, H. Q.; Shin, K.; Kim, T.; Moon, S.; McCarthy, T. J.; Russell, T. P. The Influence of Confinement and Curvature on the Morphology of Block Copolymers. *J. Polym. Sci., Part B: Polym. Phys.* **2005**, *43*, 3377−3383.

(38) Li, W.; Qiu, F.; Shi, A.-C. Emergence and Stability of Helical Superstructures in ABC Triblock Copolymers. *Macromolecules* **2012**, *45*, 503−509.

(39) Ma, M.; Titievsky, K.; Thomas, E.; Rutledge, G. Continuous Concentric Lamellar Block Copolymer Nanofibers with Long Range Order. *Nano Lett.* **2009**, *9*, 1678−1683.